Contents lists available at Science-Gate

International Journal of Advanced and Applied Sciences

Journal homepage: http://www.science-gate.com/IJAAS.html

Effect of fiber tow density and braid angle of braided basalt composite tube under crushing impact

M. Nazrul Roslan[1, 2, *], M. Yazid Yahya [2], Z. Ahmad [2], A.R. Azrin Hani [1], Iqbal Mokhtar [2]

[1]*Faculty of Engineering Technology, University Tun Hussein Onn Malaysia, 81600 Batu Pahat, Johor, Malaysia*
[2]*Centre for Composite, University Technology Malaysia, 81310 Skudai, Johor, Malaysia*

ARTICLE INFO

Article history:
Received 27 December 2015
Received in revised form
16 January 2016
Accepted 16 January 2016

Keywords:
Basalt braided
Composite tube
Energy absorption
Crass worthiness

ABSTRACT

Braiding is a process of inter-winding fiber tow in circular rotational to produce ±θ° fiber angle of braided. Braiding is one of techniques in composite fabrication which widely used in aerospace, automotive and marine applications which offers lightweight structures as well as good in absorbing impact energy. Basalt, a mineral type of natural fiber had gradually gained interest of research due to their low cost and capability in breaking domination of e-glass as reinforcement material. Basalt braided in sleeve preforms offers ease of use but diameter-angle constraints. Thus, this study had focused on the effect of fiber tow density and braid angle of under crushing response. Crushing loads crush efficiency ratio, and specific energy absorption for two type of braided basalt sleeve had been demonstrated. Failure mechanism during crushing had been observed and discussed as well. Two type of basalt braided had been sleeved over mandrels resulted different braid angle of fiber orientations before epoxy resin was used completed composite tube fabrication via brushed method and post-cured by vacuum bagging technique. Highest crushing load and stress obtained from the highest fiber tow density at ±40° braid angle. Meanwhile, sample with braid angle close to ±45° was demonstrated diamond buckling during crushing.

1. Introduction

The needs of composites in replacing metals part were drastically increased in a last few decades' studies due to their specific weight advantages as well as performance. Fibrous composites offer a custom of performance from various fracture mechanism accordance to the application because of the tailoring ability in orienting fiber to resist the specific responses. Most of common fiber used as reinforcement composite were carbon fiber, glass fiber, aramid fiber, Kevlar fiber, and one of gradually increased of interest was basalt fiber (Matsuo, 2008; Singha, 2012).

Basalt fiber originates from volcanic magma and flood volcanoes, a very hot fluid or semifluid material under the earth's crust, solidified in the open air. Singha (2012) in their short reviewed article had found that basalt is capable to withstand very high temperature and can act as fire blocking element. Basalt fibers are increasingly proposed as an alternative to glass fibers as reinforcement for composite materials, in that they combine ecological safety, natural longevity, and fire safety. In addition, basalt fiber composites have higher chemical stability, largely exceeding fiberglass as regards acid, alkali and steam resistance, which can make the former preferable over the latter e.g., in the automotive industry, where extensive use of acids is made. The properties of basalt fiber composites appear to be comparable with glass fiber composites in terms of Young's modulus, compressive and bending strength, impact force and energy (Mokhtar et al., 2015).

Textiles made by various methods such as weaving, knitting, and braiding have often been used as preforms of fiber reinforcement composite. Above all, the braiding has the characteristic that fibers are oriented continuously in any kind of shape. Braiding is an ancient textile technique with 2D braided structures are intertwined fibrous materials which capable of orienting fiber strands in 0° and ± θ° which θ/2 is define as braid angle (Nishimoto et al., 2010). The inter-lacing of the tows in the through thickness direction increases the splitting toughness and largely eliminates the delamination problem.

A numbers of research conducted proven that braid angle orientations gives significant effects to axial crushing response (Beni et al., 2014; Harte et al., 2000). Harte and Fleck (2000) observed two

* Corresponding Author.
Email Address: nazrul@uthm.edu.my

competing failure mode occurred: micro-buckling was observed for a braid angle θ < ±35°, whereas diamond shaped buckling was observed for θ > ±35°. On the other hand Gui et al. (2009) had found θ = ±30° appeared higher peak crush load compared θ = ±45° braided orientation.

Crushing mode and specific energy absorption were also found to be dependent on multiple parameter such as tube geometry, fiber type and architecture, matrix resin, testing speed, temperature, trigger and surface treatment (Priem et al., 2014). Different type of crushing mode had been introduced such as splaying, fragmentation, progressive folding, and catastrophic failure (Gui et al., 2009). Harte and Fleck (2000) had categorized the progressive folding mode into 4 type of buckling mode for braided, fiber micro-buckling, diamond shape buckling, concertina buckling, and Euler macro-buckling.

Braided tow density significantly related to yarn crimp percentage and fiber packing ratio. Due to these scenarios it is important to analysis the relation on density and braid angle for crushing response. Hence, the objective of this project is to study the effects of fiber tow density and braid angle for braided basalt fiber composite tube.

2. Experimental detail

2.1. Materials

Basalt fiber sleeve (BFS) were purchased from Siltex Co., located in Julbach, Germany in form of a 1x1 pattern of 2D biaxial braided with two different types of specifications. Fig. 1 displays braid angle definition and braided sleeve used. Table 1 shows the BFS detail of specifications. Epoxy 1006 with harderner resin type was purchased at S&N Chemical Company located in Johor, Malaysia (Table 1).

Table 1: Specifications of BFS preforms

Type	D_{nom} θ= 45°	No. of tow	Roving size
I	40 mm	100	600 Tex
II	60 mm	144	600 Tex

2.2. Sample preparation

Dry BFS was sleeved-over a mandrel with angle of $[\pm\theta^\circ]_3$ before Epoxy resin was then brushed firmly impregnated along the surface. Vacuum bagging process was used to facilitate access resin flow-out and control post-curing process. The specimen was fabricated at room temperature with 8 hours curing time. Table 2 shows the sample designations used in this project. The designation is corresponding to the number of fiber tow density and mandrel size (A and B designated for mandrel size of 42mm and 48mm diameter respectively).

After curing the composite tube was pull-out from the mandrel and it were cut according to the diameter-length ratio of 1:1.5. Top surface of sample were chamfered with 45 angle to avoid catastrophic failure during crushing test (Gui et al., 2009). Burn-out test was performed in order to get fiber weight percentage, whereby Wf = 70% had been used for this project in order to investigate better fiber tow interactions (Table 2).

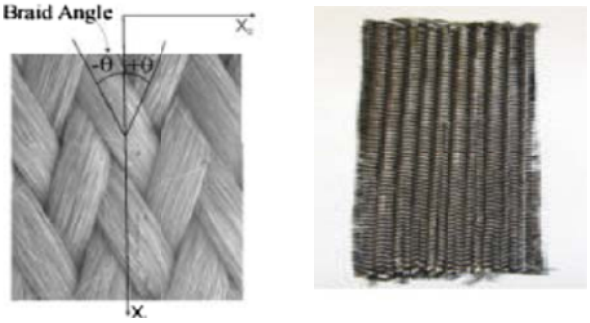

(a) (b)

Fig. 1: Braiding architecture; (a) braid angle, (b) braided sleeve

Table 2: Sample designation for this project

Specimen	D_{nom}, mm	D_i, mm	t, mm	$[\pm\theta^\circ]_3$
100A	40	42	2	45°
100B	40	48	2	60°
144A	50	42	2	30°
144B	50	48	2	40°

2.3. Crushing impact test

Axial crushing test was performed by using Universal Testing Machine, Testometric M500 supplied by Testometric Co., England. A crosshead speed of 2mm/min for 70% deflection length had been set for each specimen. The test was conducted at room temperature. Compression moduli E_{comp}, specific energy absorption (SEA), crash efficiency (CE) ratio, peak and average crush load were extracted from the load-displacement curve. While to compare the crushing response for every sample, stress-strain curve was used. Crushing mode was observed as well during crushing. SEA was computed from the area under curve (load-deflection curve) over composite weight:

$$SEA = \frac{\int F\,dx}{W} \quad (1)$$

Meanwhile CE was obtained from average load, F_{avg} over Peak load, F_{max}:

$$CE = \frac{F_{avg}}{F_{max}} \quad (2)$$

The CE value close to 1 is represent an ideal energy absorber and the structure was not in overstress condition while crushing (Priem et al., 2014).

3. Result and discussion

Table 3 displays the overall result obtained from load-deflection data. The highest peak load was acquired from specimen 144A at tubr size of D_{norm}=40mm and 144B at D_{norm} =50mm which 14.67kN and 16.68kN respectively. The total fiber tow number for specimen 144A and 144B were higher than 100A and 100B, hence the more number

of fiber reinforcement had strengthened the composite properties.

Table 3: Overall crushing result data

Specimen	Peak Load, kN	Avge. Load, kN		$E_{Comp.}$, MPa	CE	SEA, J/g	Failure mode
		Mean	Stdv.				
100A	10.40	8.974	0.88	663.7	0.86	5.58	Diamond buckling
144A	14.67	11.986	1.36	625.4	0.82	7.70	Splaying
100B	14.60	9.163	1.12	549.32	0.62	3.68	Catastrophic
144B	16.68	15.03	0.95	488.90	0.90	13.08	Diamond buckling

On the same preform of BFS comparison, increasing mandrel size had increased the braid angle. Further, loads data increased as well. Peak load for 144A and 100B obtained significantly same value even though the D_{norm} were different size.

Energy absorption is an amount of kinetic energy converted to the other form of energy. As shown in Fig. 2, the highest SEA value was obtained from the 144B specimen whereas the lowest SEA appeared on specimen 100B.

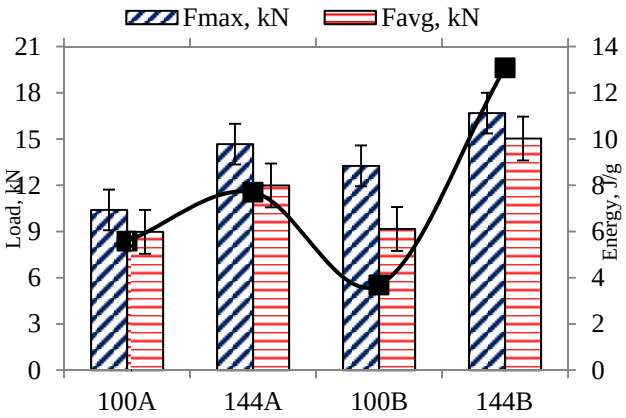

Fig. 2: Peak load, Average load, and SEA analysis result

The crushing mode observed significantly related to the SEA value whereby progressive buckling mode contributed good CE ratio. Specimen 100B had occurred catastrophic failure on crushing. In contrast, progressive folding (diamond buckling, and splaying) occurred in others specimen.

Catastrophic failure was triggered from fiber macro-buckling at middle of composite tube. As a result, sudden drop of load value happened. Fig. 3 shows the three type of failure mode occurred in this project.

Fig. 4(a) and Fig. 4(b) shows load-displacement curve for Di value of 42mm and 48mm respectively. For D_{norm}=40mm the curve trend lines shows similar pattern for both type of specimen. However, different trend line on D_{norm}=50mm specimen of 100B. Sudden drop occurred after approximate 4mm displacement length in the respective sample. As discussed earlier, it was the catastrophic failure mechanism which constant load was observed after failure before buckling started over on both top and bottom structure of the tube. On the diameter of D_{norm}=40mm, both specimen behave progressive buckling with 100A demonstrated diamond buckling and 144A specimen exhibited splaying mechanism.

(a) (b) (c)

Fig. 3: Crushing and failure mode observed during crushing; (a) diamond buckling, (b) catastrophic, (c) splaying

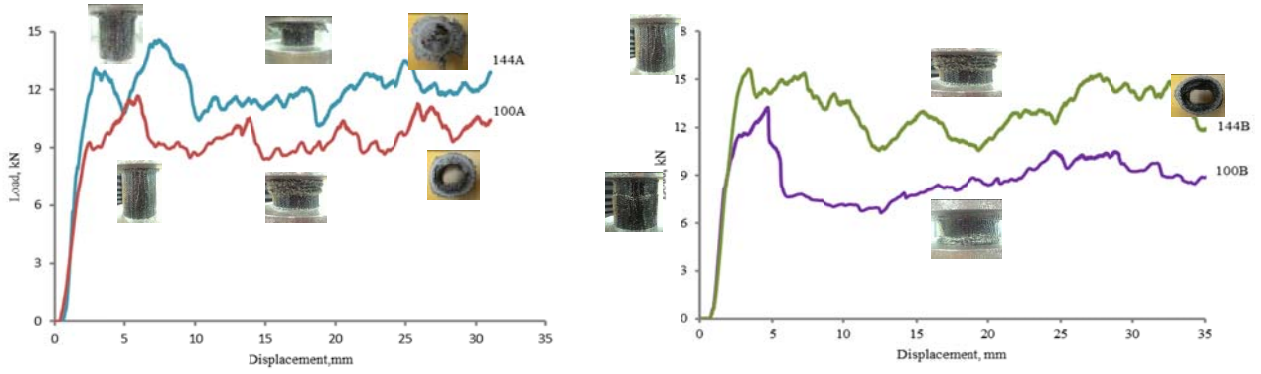

(a) (b)

Fig. 4: load-displacement curve with a failure mechanism; (a) D_{norm}=40mm, (b) D_{norm}=50mm

Progressive buckling was observed that the axial load increased rapidly to an initial peak Fmax, while micro-fracture failure occurred and small inter-laminar and intra-laminar cracks were formed at the

location of the chamfer trigger. The lamina bundles near the chamfer end exhibited bending inwards and could fracture at the base of lamina bundle, leading to a sharp drop in the crushing load. For splaying mode, crack growth was the principal energy-absorption mechanism, accompanied with the lamina bundles bending and frictional effects between the platen, fronds, debris wedge and adjacent lamina. However, diamond buckling mode, the primary energy-absorption mechanism was fracture of the triggering micro-cracking of matrix bundles with inter-laminar and then after progressive buckling on the tube circumference.

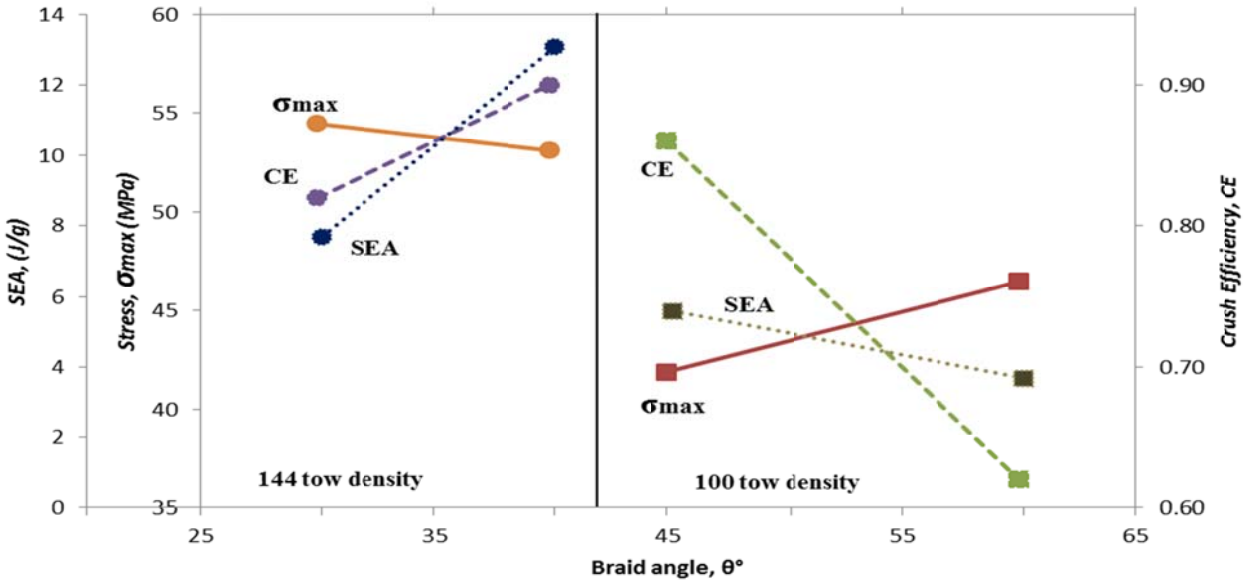

Fig. 5: Maximum stress, specific energy absorption and crush efficiency ratio lines vs. braid angle

As stated in specimen preparation section, two different sizes of mandrel and braided tow densities had been used. Therefore, 144 tow density produced low angle of braid angle on D_{norm}=40mm and D_{norm}=50mm with θ=30° and θ=40° braid angle respectively. While, 100 tow density BFS type had produced high braid angle which ±45° and ±60° respectively. In other words, 144 tow densities produced low braid angle with the same mandrel size of 100 tow density. Hence to further observe the relation between braided densities and braid angle.

Fig. 5 shows stress values, specific energy absorption and crush efficiency over different of braid angle. The highest maximum stress exhibited on 144 tow densities at +30° braid angle. Meanwhile, the lowest maximum stress performed on the 100 tow density at ±45° braid angle. It can be said that low braid angle performed high stress value because of percentage fiber were increased towards longitudinal axis when braid angle decreased. The same scenario observed on previous studies (Falzon and Herszberg 1998).

Specific energy absorption, SEA performed highest on 144 tow density at ±40° braid angle and decreasing over braid angle on 100 tow density. The same trends occurred on crush efficiency, CE ratio lines. The highest CE value was also obtained on 144 tow densities at ±40° braid angle. CE ratio value represented tube stability in absorbing energy during crushing. Low CE value can be considered as poor energy absorber in dissipating energy over length of impact displacement.

Braid angle, ±60° had obtained the lowest CE value. With high fiber fraction on the composite had lead the dependent of fiber itself to resist external load. High braid angle contributed to high fiber crimp on the wall (Potluri, 2006). Hence, tow thickness decrease and affected buckling length. As a result, catastrophic failure happened due to buckling was started in the middle of tube not at chamfered point. Similar scenario had been reviewed by (Ayranci and Carey, 2008).

Fig. 5 also displays, CE ratio had been seen well at close to ±45° braid angle. (Ayranci and Carey 2008) had reviewed that most of researchers proven that the optimum angle which can withstand multiple direction of external load was ±45° tow orientation angle due to their symmetrical geometry. Instead of good in shear, torsional and stiffness, it also increase transverse moduli, transverse strength, damage tolerance, and dimensional stability (Ayranci and Carey 2008).

4. Conclusion

Effects of number of tow density and braid angle for basalt braided composite tube under crushing impact had successfully demonstrated. The highest crushing load and stress was obtained from high fiber tow density and decreased along braid angle increased. At the same fiber weight fraction, Wf% was observed that the more fiber tow density had performed better strength and energy absorption compared with less number of tow density.

Three type of crushing mode had been found in this project which was diamond buckling, splaying mode and catastrophic mode. Braid angle close to ±45° revealed diamond buckling on progressive

folding, while ±30° braid angle exhibited splaying mode during crushing. However ±60° braid angle had catastrophic failure due to fiber crimp. SEA value performed highest upon near ±40° and decreased towards ±60° braid angle. CE ratio value demonstrated same trends as well. Braid angle near of ±45° exhibited stability on energy dissipation proven by CE value and crushing failure mode.

Thus, in material braided sleeve design selection for crashworthiness, its recommended that product designer not only select based on "diameter to use" but they should consider the higher fiber tow density that can be used as well to fit the diameter to get the best strength and energy absorption. Further, second priority was the braid angle should in range of ±40° to ±50° so to get good CE ratio and progressive buckling.

Acknowledgement

This project was supported by 'Skim Latihan Akademik Bumiputera' (SLAB) from Ministry of Education Malaysia.

References

Ayranci C and Carey J (2008). 2D braided composites: a review for stiffness critical applications. Composite Structures, 85(1): 43-58.

Beni ZT, Johari MS and Ahmadi MS (2014). Comparison of the Post-Impact Behavior of Tubular Braided and Filament Wound Glass/Polyester Composites under Compression. Journal of Engineered Fibers and Fabrics, 9(2): 140-145.

Falzon PJ and Herszberg I (1998). Mechanical performance of 2-D braided carbon/epoxy composites. Composites science and technology, 58(2): 253-265.

Gui LJ, Zhang P and Fan ZJ (2009). Energy absorption properties of braided glass/epoxy tubes subjected to quasi-static axial crushing. International Journal of Crashworthiness, 14(1): 17-23.

Harte AM and Fleck NA (2000). Deformation and failure mechanisms of braided composite tubes in compression and torsion. Acta Materialia, 48(6): 1259-1271.

Harte AM, Fleck NA and Ashby MF (2000). Energy absorption of foam-filled circular tubes with braided composite walls. European Journal of Mechanics-A/Solids, 19(1): 31-50.

Mokhtar I, Yahya MY, Kader A, Saman A and Abu Hassan S (2014). Energy Absorption of Basalt Filament Wound Rectangular Tubes: Experimental Study. In Applied Mechanics and Materials (711: 201-205). Trans Tech Publications.

Nishimoto H, Ohtani A, Nakai A and Hamada H (2010). Generation and prediction methods for circumferential distribution changes in the braiding angle on a cylindrical braided fabric. Proceedings of the Institution of Mechanical Engineers, Part L: Journal of Materials Design and Applications, 224(2): 71-78.

Potluri P, Manan A, Francke M and Day RJ (2006). Flexural and torsional behavior of biaxial and triaxial braided composite structures. Composite Structures, 75(1): 377-386.

Priem C, Othman R, Rozycki P and Guillon D (2014). Experimental investigation of the crash energy absorption of 2.5 D-braided thermoplastic composite tubes. Composite Structures, 116: 814-826.

Singha K (2012). A short review on basalt fiber. International Journal of Textile Science, 1(4): 19-28.

Matsuo T (2008). Fibre materials for advanced technical textiles. Textile Progress, 40(2): 87-121.